Acta Crystallographica Section B
Structural Science
ISSN 0108-7681

addenda and errata

Structures of mono-unsaturated triacylglycerols. II. The β_2 polymorph. Corrigendum

Jan B. van Mechelen,* Rene Peschar and Henk Schenk

University of Amsterdam, HIMS/FNWI/Kristallographie, Valckenierstraat 65, 1018 XE Amsterdam, The Netherlands

Correspondence e-mail: janvm@science.uva.nl

A replacement Fig. 3 to the paper by van Mechelen *et al.* (2006), *Acta Cryst.* B**62**, 1131–1138 is given.

Fig. 3 in the article by van Mechelen *et al.* [(2006*b*), *Acta Cryst.* B**62**, 1131–1138] is actually a duplicate of Fig. 3 from van Mechelen *et al.* [(2006*a*), *Acta Cryst.* B**62**, 1121–1130]. The correct figure is given here.

References

Mechelen, J. B. van, Peschar, R. & Schenk, H. (2006*a*). *Acta Cryst.* B**62**, 1121–1130.
Mechelen, J. B. van, Peschar, R. & Schenk, H. (2006*b*). *Acta Cryst.* B**62**, 1131–1138.

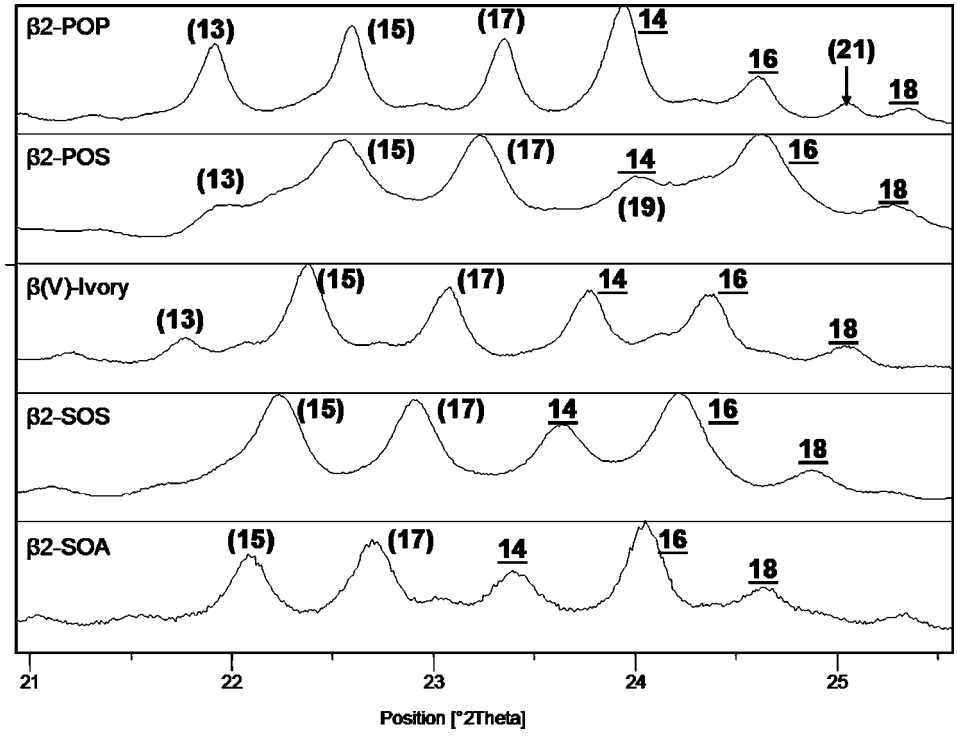

Figure 3
Higher-angle part of Fig. 2 showing the differences between the β_2 patterns. (1, k, −1) peaks are labeled (k) and (0, k, 2) peaks are labeled underscore k.

 doi:10.1107/S0108768106055753

Acta Crystallographica Section B
Structural Science
ISSN 0108-7681

Structures of mono-unsaturated triacylglycerols. II. The β_2 polymorph

Jan B. van Mechelen,* Rene Peschar and Henk Schenk

University of Amsterdam, HIMS/FNWI/Kristallographie, Valckenierstraat 65, 1018 XE Amsterdam, The Netherlands

Correspondence e-mail: janvm@science.uva.nl

Received 26 July 2006
Accepted 12 September 2006

An improved crystal structure model has been established for the β_2 polymorph of the symmetric mono-unsaturated triacylglycerol 1,3-distearoyl-2-oleoylglycerol (SOS) and the equivalent β-V polymorph of Ivory Coast cocoa butter. In addition, the crystal structures of the β_2 polymorphs are reported for the triacylglycerols 1,3-dipalmitoyl-2-oleoylglycerol (POP) and 1-palmitoyl-2-oleoyl-3-stearoylglycerol (POS), which are, together with SOS, the major components of cocoa butter, and that of 1-stearoyl-2-oleoyl-3-arachidoylglycerol (SOA). The existence of β_2-POS and β_2-SOA has not been previously reported in the literature. All structures have been solved from high-resolution laboratory or synchrotron powder diffraction data with the direct-space parallel-tempering program *FOX* and refined with the Rietveld module of *GSAS*. All compounds crystallize in similar monoclinic unit cells (*Cc*) with very long *b* axes (> 127 Å). The oleic chains are packed together and sandwiched between saturated chain layers, forming acyl-chain three-packs. An analysis of the β_2 polymorphs and β_1 polymorphs [van Mechelen *et al.* (2006). *Acta Cryst.* B**62**, 1121–1130] shows that they contain the same three-packs and differ only in the symmetry relation between the three-packs. The three-pack build-up provides an explanation of the mechanism of the phase transition that causes the formation of fat bloom on dark chocolate.

1. Introduction

The polymorphic phase transitions of fats and their constituent triacylglycerols (TAGs) in consumer products are generally unwanted because they lower the quality. Chocolate, for example, contains cocoa butter that, with the common industrial tempering process, usually crystallizes in the second-highest melting phase, the β_2 phase, which is better known as β-V. Inevitably a $\beta_2 \rightarrow \beta_1$ phase transition takes place in cocoa butter, commonly referred to as the β-V $\rightarrow$ β-VI transition that brings forth fat bloom on chocolate. It has been hypothesized that this and other polymorphic phase transition processes involve (re-) packing of the long fatty-acid acyl chains and/or layers. To establish the precise mechanism of such phase transition processes, crystal-structure models are indispensable.

In the previous paper (Part I; van Mechelen *et al.*, 2006) we presented the crystal structures of the β_1 polymorph of several monounsaturated TAGs and the (similar) β-VI polymorph of cocoa butter. All these models were obtained using direct-space search techniques and high-resolution laboratory and synchrotron powder diffraction data. The experience gained with the structure determination and refinement of the β_1

polymorphs led us to re-analyze an earlier reported structure determination of the β_2 polymorph of SOS and the (similar) β-V polymorph of Ivory Coast cocoa butter (Peschar *et al.*, 2004). In this paper we present a novel β_2 crystal-structure model. Using high-resolution powder diffraction data, we have been able to solve the β_2 polymorph structures of 1,3-dipalmitoyl-2-oleoylglycerol (POP), 1,3-distearoyl-2-oleoylglycerol (SOS) and the β-V polymorph of Ivory Coast cocoa butter. We also solved the β_2 polymorph crystal structures of 1-palmitoyl-2-oleoyl-3-stearoylglycerol (POS) and 1-stearoyl-2-oleoyl-3-arachidoylglycerol (SOA). To our knowledge, the latter two are novel polymorphs whose existence has not been previously reported in the literature. The novel β_2 structural model will be discussed in relation to the model of the β_1 polymorphs and provide an explanation of the mechanism of the phase transition that causes the formation of fat bloom on dark chocolate.

2. Experimental methods

2.1. Samples, sample preparation and data collection

Samples of POP, SOS and POS ($\sim$ 97.6%), and SOA ($\sim$ 97.7%) were obtained from Unilever Research Laboratorium (Vlaardingen, The Netherlands) and Unilever R&D Colworth (Sharnbrook, UK). Ivory Coast cocoa butter was obtained from ADM (Koog a/d Zaan, The Netherlands). The materials used for this publication (all racemic mixtures) were from the same batches that were used for the β_1 polymorphs presented in Part I (van Mechelen *et al.*, 2006). Samples of POP, SOS and POS, as their β_1 polymorphs, were placed into glass capillaries and carefully heated up to their melting points. After melting all the solid material (established visually), the melt was cooled to 296 K to grow the β_2 polymorph. The Ivory Coast cocoa butter was treated in the same way to obtain a pure β_2 polymorph. The SOA sample was originally delivered as the β_1 polymorph. To our surprise, after a couple of years in storage in the laboratory (most of the time in the refrigerator at 283 K), it turned out to be in the β_2 phase. The β_2-SOA powder was then placed in a glass capillary for data collection.

β_2-POS was crystallized by the same treatment used for the growth of other β_2 polymorphs. The original powder, a pure β_1 polymorph, was heated to just above the melting point at 313 K and subsequently cooled down to 296 K, at which temperature the β_2 polymorph readily crystallized. When stored at 295 K the β_2 polymorph converts at least partly to β_1 over several months. To explain the unexpected crystallization of this novel β_2-POS polymorph additional melt and crystallization experiments were carried out.

All samples were checked for the coexistence of more than one polymorph on the in-house X'pert Pro-alpha1 diffractometer (PANalytical, Almelo, The Netherlands) before carrying out a full data collection. The β_2-POS sample was measured at the high-resolution powder station of beamline BM01b at the ESRF (Grenoble, France). For β_2-POP and β-VI-Ivory Coast, data was collected at the high-resolution powder station ID31 at the ESRF (Grenoble, France). The β_2-SOS and β_2-SOA samples were measured on the in-house X'pert Pro-alpha1 diffractometer. This diffractometer was equipped with a sealed Cu X-ray tube, 0.01 rad primary and secondary Soller slits and a hybrid monochromator that produces a parallel Cu $K\alpha_1$ X-ray beam. The X'celerator strip detector was used at its maximum active length of 2.17° 2θ. Data collection conditions for each of the samples are given in Table 1.[1] The capillaries were spun in all cases. The continuous scans were binned with a step size of 0.005° 2θ for the BM01b and ID31 data and a step size of 0.008° 2θ for the X'pert Pro-alpha1 data.

Some of the samples appeared to have a small impurity line of unknown origin between the first and the second reflection. This peak has been excluded from the refinement in all cases (see Table 1).

Melting points have been determined with a Linkam DSC600 (Linkam Scientific Instruments Ltd, Tadworth, UK). Samples were heated at 2 K min^{-1}. The melting points given in Table 1 are the temperatures at which the melting peaks are at a maximum. The DSC traces showed no evidence for the coexistence of more than one phase.

2.2. Indexing, model building, structure determination and refinement

The indexing of powder diffraction patterns of mono-unsaturated TAGs is a complicated process, as already explained in our publication (Part I: van Mechelen *et al.*, 2006) about the β_1 structures of SatOSat'-type compounds. For the β_2 polymorphs in the present publication we did not start the indexing from scratch, but used the unit cells of the corresponding β_1 structures instead. With the help of the program *Chekcell* (Laugier & Bochu, 2001), in all cases good indexing was found by the alternate coupling of the appropriate Miller indices to peak position markers in the observed diffraction pattern and unit-cell refinement. The most probable space group (*Cc*) was found with the help of the structure solution program *FOX* (Favre-Nicolin & Černý, 2002) in the following way. The asymmetric unit (*Z*-matrix description) of a TAG β_1 structure was placed in the refined β_2 unit cell and powder patterns were subsequently calculated for various monoclinic space groups with a fourfold general position, and compared with the experimental β_2 data.

The model has been optimized in *Cc* with the parallel tempering mode of Fox and a *Z*-matrix description of the molecule. The same settings of degrees of freedom were used as in the structure solution of the β_1 structures, *i.e.* rotation and translation of the molecule and gradual inclusion of torsion-angle flexibility at the glycerol group.

The Rietveld structure refinement was carried out with the program *GSAS* (Larson & Von Dreele, 1987) and the refinement strategy was essentially the same as for the β_1 structures, including the application of soft distance, angle and planar

[1] Supplementary data for this paper are available from the IUCr electronic archives (Reference: DR5012). Services for accessing these data are described at the back of the journal.

Table 1
Experimental and structural details of β_2-structures.

	β_2-POP	β_2-SOS	β_2-POS	β_2-SOA	β-V Ivory
Crystal data					
Chemical formula	$C_{53}H_{100}O_6$	$C_{57}H_{108}O_6$	$C_{55}H_{104}O_6$	$C_{59}H_{112}O_6$	$C_{54.96}H_{108}O_6$
M_r	833.38	889.48	861.43	917.54	865.46
Cell setting, space group	Monoclinic, *Cc*	Monoclinic, *Cc*	Monoclinic, *Cc*	Monoclinic, *Cc*	Monoclinic, *Cc*
Temperature (K)	280	298	250	298	280
a, *b*, *c* (Å)	5.447 (1), 122.62 (2), 8.220 (1)	5.440 (1), 130.30 (1), 8.221 (1)	5.424 (1), 126.53 (2), 8.121 (2)	5.438 (1), 135.29 (1), 8.213 (2)	5.442 (1), 127.64 (1), 8.214 (2)
β (°)	88.78 (1)	88.75 (1)	88.51 (2)	88.64 (2)	88.69 (9)
V (Å^3)	5444.1 (2)	5825.8 (4)	5571.5 (4)	6040.1 (1)	5704.0 (4)
Z	4	4	4	4	4
D_x (Mg m^{-3})	1.017	1.014	1.027	1.015	0.997
Radiation type	Synchrotron	Cu $K\alpha_1$	Synchrotron	Cu $K\alpha_1$	Synchrotron
Specimen form, colour	Cylinder (particle morphology: solid fat), white	Cylinder (particle morphology: solid fat), white	Cylinder (particle morphology: solid fat), white	Cylinder (particle morphology: powder), white	Cylinder (particle morphology: solid fat), yellowish white
Specimen size (mm)	5 × 1 × 1	12 × 1 × 1	20 × 1 × 1	12 × 0.7 × 0.7	5 × 1 × 1
Specimen preparation temperature (K)	302	295	302	295	295
Data collection					
Diffractometer	ESRF ID31	X'pertPro-Alpha1	ESRF BM01b	X'pertPro-Alpha1	ESRF ID31
2θ (°)	$2\theta_{min}$ = 0.005, $2\theta_{max}$ = 58.0	$2\theta_{min}$ = 0.52, $2\theta_{max}$ = 60.0	$2\theta_{min}$ = 0.136, $2\theta_{max}$ = 30.48	$2\theta_{min}$ = 0.79, $2\theta_{max}$ = 50.0	$2\theta_{min}$ = 0.003, $2\theta_{max}$ = 77.96
Refinement					
R factors and goodness-of-fit	R_p = 0.067, R_{wp} = 0.099, R_{exp} = 0.024, S = 4.37	R_p = 0.038, R_{wp} = 0.058, R_{exp} = 0.016, S = 3.86	R_p = 0.079, R_{wp} = 0.086, R_{exp} = 0.018, S = 5.07	R_p = 0.063, R_{wp} = 0.085, R_{exp} = 0.032, S = 2.70	R_p = 0.056, R_{wp} = 0.065, R_{exp} = 0.021, S = 3.15
λ (Å)	1.24993	1.54059	0.79948	1.54059	1.24993
Excluded region(s)	No	1.56–1.864	0.985–1.075	0.65–0.685	1.36–1.8
No. of parameters	505	550	525	561	548
H-atom treatment	Constrained to parent site	Constrained to parent site	Constrained to parent site	Constrained to parent site	Constrained to parent site
$(\Delta/\sigma)_{max}$	0.04	0.15	0.54	1.92	0.09

restraints, and rigid bodies. In the model for the Ivory Coast cocoa butter the occupancy of the last two C atoms of the saturated chains was fixed at 0.5, in view of the experience with occupancy refinement of the cocoa butter β_1 models. The experimental details for all compounds are listed in Table 1. A schematic drawing of the TAG molecules with atom and chain labeling is given in Fig. 1. The preferred orientation (PO) was corrected for by the March–Dollase function (March, 1932; Dollase, 1986) for β-V Ivory Coast (axis: [010] ratio = 1.04 correction range: min = 0.87, max = 1.07). For the other samples no significant PO was found. The final results of the refinements are shown in the figures given in the supplementary material.

3. Results and discussion

3.1. Data collection

Fig. 2 gives an overview of the experimental diffraction patterns of all the samples, with the 2θ scale being converted to the same scale (2θ, Cu $K\alpha_1$) and ordered from top to bottom with increasing length of the *b* axis. As for the β_1 structures, the low-angle parts of the diffraction patterns ($2\theta < 10°$, Cu $K\alpha_1$ radiation) are dominated by the (0*k*0) reflections and are quite similar.

The synchrotron pattern upon which the $P\bar{1}$ β_2-SOS structural model (Peschar *et al.*, 2004) is based has also been included in Fig. 2. In spite of its overall good quality, it has

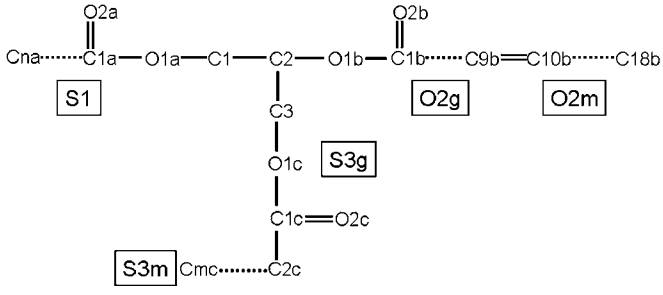

Figure 1
Chemical structure diagram of SatOSat'-type TAGs. The structural subscripts *m* and *n* (= 16, 18, 20) label the atom numbers while S1, S3*g*, S3*m*, O2*g* and O2*m* label the saturated acyl chain and the acyl chain parts. *g* and *m* denote the glycerol and methyl sides, respectively.

been established that the beam-stop partly obstructed the intensity of the (010) and (020) reflections (for the cell listed in Table 1). Although this problem was recognized at that time and did not seem to influence the model seriously, our recent experience with solving β_2 (this paper) and β_1 polymorphs (Part I; van Mechelen *et al.*, 2006) has led to the opinion that correct low-angle intensities are essential to obtain the most realistic structural model.

Fig. 3 zooms in on part of the fingerprint area of Fig. 2 and the reflections have been marked with their Miller indices. The reflections shift to lower angles with increasing length of the *b* axis and also change in relative intensity. This effect is most clearly visible for the two outermost reflections: on increasing the length of the *b* axis the intensity of the $(\bar{1},13,1)$ reflection gradually disappears, while that of the (0,16,2) reflection increases. This effect can be attributed to a change in orientation of the chain layers relative to the crystal planes as a function of the length of the *b* axis.

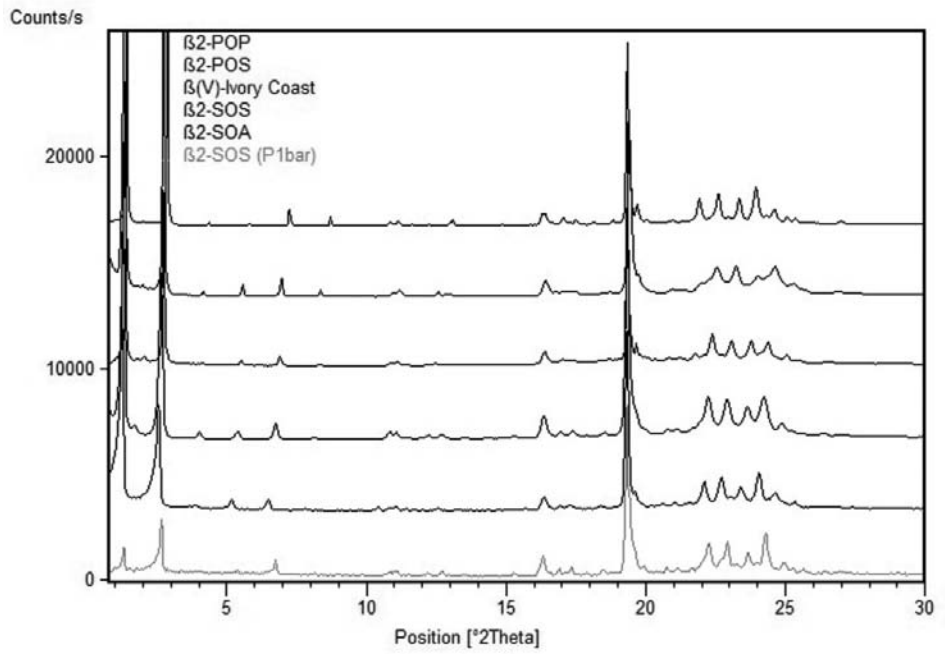

Figure 2
Overview of β_2 diffraction patterns with the 2θ scale converted to Cu $K\alpha_1$ radiation. The bottom pattern was used for the structure determination of the $P\bar{1}$ model (Peschar *et al.*, 2004).

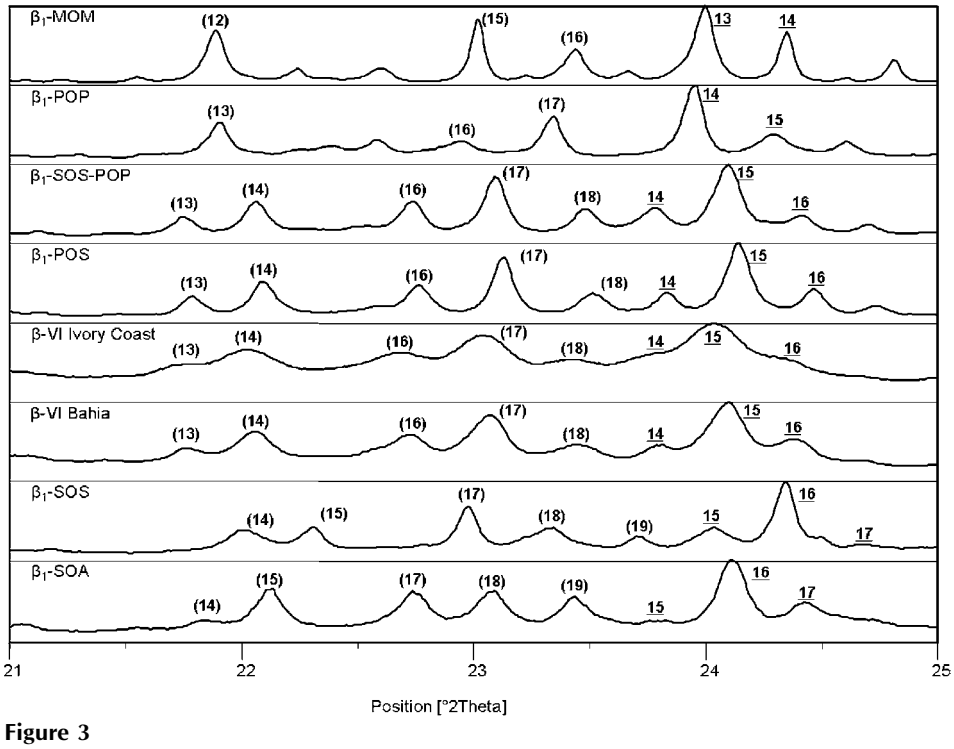

Figure 3
Higher-angle part of Fig. 2 showing the differences between the β_2 patterns. $(1, k, -1)$ peaks are labeled (k) and $(0, k, 2)$ peaks are labeled underscore k.

3.2. Anisotropic cell-parameter contraction

Besides the room-temperature data of β_2-SOS, a data set collected at 115 K at the BM01b station was also available. Unfortunately, this sample appeared to contain too much of the β_1 polymorph to use for structure refinement, but it was still possible to extract the β_2 unit-cell dimensions. A comparison of the unit-cell parameters of both data sets (Table 2) reveals an anisotropic contraction as the temperature is lowered with the second shortest (*c*) axis being influenced the most. This anisotropic behaviour is also the reason for the relatively small *c* axis of β_2-POS, as these data were collected at a temperature which was 40 K lower than that of the other four samples. This difference in temperature hampers the comparison of the cell dimensions within the series.

3.3. The novel β_2-POS and β_2-SOA polymorphs

The occurrence of the novel β_2-POS polymorph is attributed to the presence of a small amount of a high-melting crystalline phase in the original POS batch that probably acts as a seeding template for β_2 crystallization. Additional experi-

Table 2
Indexed unit-cell parameters of β_2-SOS.

	Literature†	Literature‡	Indexed§	Indexed§	Indexed§	Indexed§
Station	BM01b	Calculated	BM01b	BM01b	X'pert	BM01b
T (K)	273	–	273	273	298	115
a (Å)	5.462	5.462	5.46	5.455	5.45	5.44
b (Å)	65.36	130.62	65.50	130.78	130.35	130.22
c (Å)	8.211	8.211	8.20	8.215	8.225	8.03
α (°)	89.72	89.77	89.75	90	90	90
β (°)	88.83	88.83	88.80	88.75	88.85	88.08
γ (°)	87.78	90.17	87.75	90	90	90
V (Å^3)	2928.4	5856.7	2930	5859	5826	5685
M_{20}	13		22	20	21	15

† Cell parameters of refined model from Peschar *et al.* (2004) ‡ Transformed from cell parameters of refined model from Peschar *et al.* (2004) using $a' = a$, $b' = -a + 2b$, $c' = c$. § This work, indexed with the program *LSQDETC* (see Part I; van Mechelen *et al.*, 2006).

ments revealed that if the POS sample is heated above 321 K, the β_1 polymorph no longer crystallizes. A possible explanation is that beyond this temperature the crystal lattice of the high-melting phase is destroyed, after which this material remains dissolved in the POS liquid and does not crystallize as a separate seeding phase. Fatty-acid methyl ester analyses showed the POS sample to contain 0.1% of a fully saturated C20 chain and HPLC indicated the presence of 0.3% of a C58 compound. In view of this, the most likely candidate is β_1-AOA (C58) that has T_m = 321 K (Koyano *et al.*, 1990), although this also implies that β_1 seeds can instigate β_2 crystallization. The seeding effect of the addition of a few tenths of a percent of a Sat-O-Sat type TAG to chocolate is well known (Koyano *et al.*, 1990).

The conversion of the SOA powder from the β_1 polymorph into the β_2 polymorph was a very slow process. The complete conversion took $\sim$ 5 years. Attempts to obtain the β_1 polymorph by tempering the β_2 polymorph failed and crystallization from an acetone solution at room temperature only produced the β_2 polymorph. The surprising β_2 preference of this SOA sample may be related to the presence of impurities such as AOA ($\pm$ 0.7%) and SOS ($\pm$ 1.2%). The stabilization of lower-melting polymorphs by impurities has been previously reported (Lovegren *et al.*, 1976; Lovegren & Gray, 1978). More experimental work is needed to verify this hypothesis.

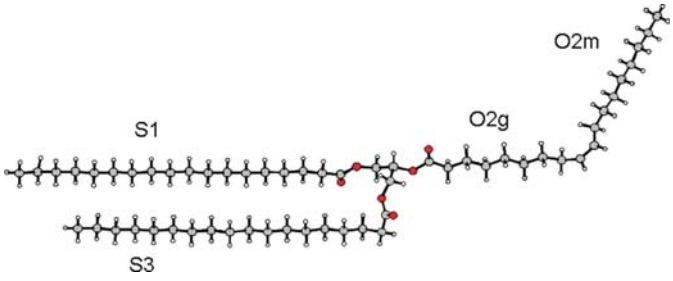

Figure 4
Conformation of the β-V Ivory Coast average molecule.

3.4. Indexing, structure determination and refinement of the β_2 polymorphs

Surprisingly, for all β_2 samples discussed in this paper, the powder patterns calculated with the β_2 cells and β_1 coordinates showed a remarkable similarity with the β_2 patterns observed in the space group Cc, but not in other monoclinic space groups with Z = 4 and a single molecule in the asymmetric unit. Since the complete intensity patterns were well covered by the calculated reflection positions and complied with the space-group extinctions of Cc, this space group was taken as the most likely candidate. The similarity of the unit cells and the single molecule in the asymmetric unit in both cases suggests a close relationship between the β_1 and β_2 structures.

If the triclinic unit cell of the $P\bar{1}$ β_2-SOS structure is transformed to a cell that is twice as large with $b' = -a + 2b$, an almost monoclinic cell is obtained with dimensions that are very close to those of the refined monoclinic cell of β_2-SOS (Table 2), taking into account that the temperatures at data collection differed by 303 K. Before the monoclinic β_1 cells with the double-length b axis had been found, this type of solution had not been considered for the β_2-SOS and β-V cocoa butter polymorphs, in particular because the indexing figure of merit, M_{20}, is better for the $P\bar{1}$ solution (Table 2). It should be noted that the unit-cell parameters of the refined structure (Table 1) differ somewhat from the original values obtained in the indexing process (Table 2) and the M_{20} indexing figure of merit is also lower for cell parameters of the refined structure. The reason is that in the current version of *GSAS* the asymmetry of the peaks can be fitted satisfactorily only if changes in the unit-cell parameters are allowed for.

A second reason why the new β_2 model is more plausible is that the preferred orientation in the $P\bar{1}$ model was assumed to

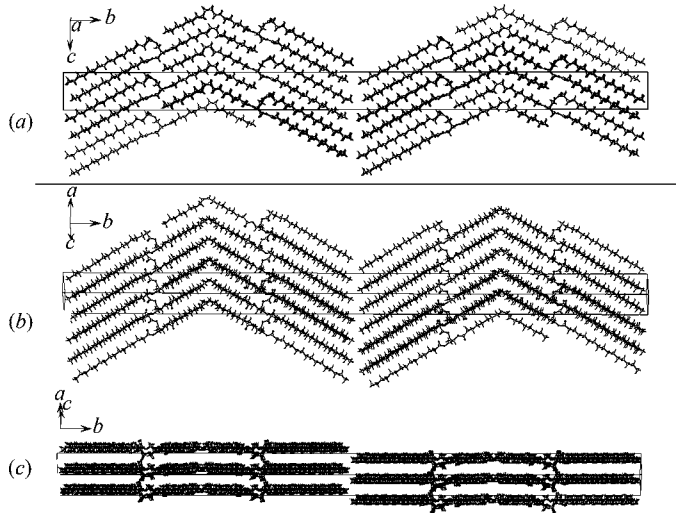

Figure 5
Packing of β_2-POS. (*a*) View down the *a* axis showing the (0,16,2) layers; (*b*) view parallel to ($\bar{1}$01) showing the ($\bar{1}$,17,1) layers; (*c*) view parallel to (101) showing the shifted molecule layers.

be present at the stage of model finding with *FOX* with [111] as the PO direction. Although on other occasions such an assumption has been successful, it seems that this assumed PO compensated for the too low intensity of the (111) peak in the $P\bar{1}$ structural model and hid its imperfections.

4. The novel β_2 polymorph crystal-structure model

4.1. Conformation of TAGs

The conformation of the TAG molecules in the β_2 (and β-V) crystal structures is identical to that of the β_1 polymorphs, and to that in the previous $P\bar{1}$ model: a flat conformation, parallel S1 and S3 chains with a *gauche* bend in S3 and a skew–*cis*–skew' geometry at the double bond in the O2 chain. More details can be found in Part I (van Mechelen *et al.*, 2006) and in Fig. 4, β-V, in which Ivory Coast is given as an example. These conformational characteristics are in full agreement with other physical data in the literature. From FT-Raman carbonyl stretching data, Sprunt *et al.* (2000) inferred that two of the three carbonyl groups in β_1-SOS as well as β_2-SOS should be in a *trans* conformation and one in a *gauche* conformation. The carbonyl conformations in our β_1 and β_2 structures are in line with the findings of Sprunt *et al.* (2000). The skew–*cis*–skew' conformation at the C=C bond has also been suggested by Yano *et al.* (1993) for both β polymorphs based on FT-IR results. As with the β_1 polymorphs, there is no significant difference between the β_2 conformations of symmetric and asymmetric TAGs.

In view of the resolution of the data, a detailed analysis of the glycerol torsion angles has not been carried out.

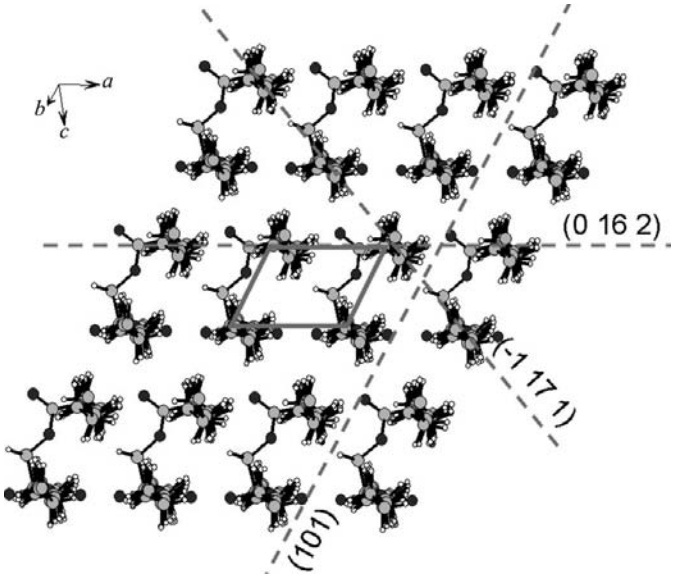

Figure 6
View parallel to the chain direction of half a POS three-pack layer cut at the double bond zone. The O and S chains are well aligned and form a $M_{\|}$ subcell.

4.2. Build-up and stacking of 'three-packs'

As in the β_1 polymorphs (space group $P2_1/n$), in the *Cc* space group of the β_2 polymorphs the same two symmetry operators (x, y, z) and $(x+\frac{1}{2}, -y+\frac{1}{2}, z+\frac{1}{2})$ define a three-pack that consists of an unsaturated zone which is sandwiched by two saturated ones (Fig. 5). Within the resolution of the data, the β_1 and the β_2 polymorphs have an identical molecular conformation and three-pack build-up. The sole difference between the β_1 and the β_2 crystal-structure models resides in the different stacking of neighbouring three-packs: in β_1 they are related by inversion centers, while in the β_2 polymorph they are related by the *Cc* lattice-centering operator $(\frac{1}{2}, \frac{1}{2}, 0)$. The saturated chains of adjacent three-packs in the β_2 polymorphs are inclined towards each other and form a terrace-type methyl end-plane (Fig. 5*a*). The flat molecules are packed in layers and the layers of molecules of adjacent three-packs are shifted relative to each other (Fig. 5*c*). De Jong *et al.* (1991) already speculated about the existence of a simple layer-stacking difference between β_1 and β_2, although they believed that only single-crystal diffraction could give an answer.

4.3. Subcell

When the three-packs are cut in half at the C9*b*=C10*b* bond, a view parallel to the chain direction (Fig. 6) shows a good alignment of the S and O chains that together form an $M_{\|}$ subcell. This subcell differs from subcells proposed for the S and O chains in the literature (Sato *et al.*, 1989). Yano *et al.* (1993) judged the FT-IR data of β_2-SOS to be inconclusive regarding the subcell structure and attributed this to an incomplete polarization of the β_2-SOS structure. The inhomogeneity of β_2, also mentioned by Yano *et al.* (1993) although assumed to be less plausible, seems to be a more likely explanation than incomplete polarization. The reflections in the fingerprint area of the β_2 TAGs are always broader than those of the β_1, thus complying with an enhanced crystallinity of the latter.

4.4. Fingerprint area interpretation

The directions of the main crystal planes in a view parallel to the chain direction (Fig. 6) have been marked with their Miller indices and correspond to reflections in the enlarged fingerprint area (Fig. 5), except (101). The position of this latter plane (Fig. 6) is between the layers of molecules and coincides with the *b* axis in Fig. 5. The (111) plane that causes the β characteristically dominant diffraction maximum in the fingerprint area (Fig. 2, 19.5° 2θ) is slightly tilted relative to (101) and cuts the shifted molecular layers of two adjacent three-packs. Views along the *a* axis and parallel to $(\bar{1}01)$ (Figs. 5*a* and *b*) show the layered packing of the individual acyl chains along the same directions as marked in Fig. 6. The fingerprint area contains two classes of reflections: $(0k2)$ with k = 14–20 and $(\bar{1}k1)$ with an odd k ranging from 13 to 21. Both types of lattice planes are slightly inclined towards each other and their intensity fades away when the lattice plane direction deviates more from the chain direction.

4.5. Methyl end-plane packing and melting points

The methyl end-planes in the β_1 and β_2 structures are essentially the same, although the interaction at the end-plane between the adjacent three-packs is different owing to the parallel (β_1) and inclined (β_2) orientation of the S chains, respectively. This difference complies with the polarized-microprobe FT-IR results of β_1- and β_2-SOS (Yano *et al.*, 1993). In β_1-SOS the $\upsilon_{as}(CH_3)$ stretching showed a strong and sharp polarization-dependent peak, whereas in β_2-SOS this peak was broader and less polarization-dependent.

In view of the identical molecular TAG conformation and three-pack built-up in the β_1 and β_2 polymorphs, the lower melting points of the β_2 polymorph can only be explained by stacking differences and/or reduced van der Waals interactions at the methyl end-plane. For example, in the case of the monoacid saturated TAGs, the lower melting points of the odd-numbered series members could be explained by a less dense packing at the methyl end-plane, as exemplified by their relatively larger occupiable volume (= volume large enough to fit an atomic probe; Van Langevelde, Van Malssen *et al.*, 2001; Helmholdt *et al.*, 2002). However, calculation of the occupiable volume at the methyl end-plane with the program *Cerius*^{2} (Molecular Simulations Inc., 2000) using a probe of 1.6 Å and atomic van der Waals radii for the β_1 polymorphs (paper I) and β_2 polymorphs (this paper) of POP, SOS, POS and SOA did not result in significantly different volumes, although the lack of atomic resolution prevents us from drawing further conclusions from this observation.

An analysis of the results shows that a reduction of the melting point is accompanied by an enlargement of the longest (observable) *d* spacing. This observation holds for:

(i) the odd-numbered monoacid saturated TAGs *versus* the even-numbered ones,

(ii) the monounsaturated β_2 polymorphs discussed in this paper *versus* the β_1 polymorphs from Part I (van Mechelen *et al.*, 2006) and

(iii) the asymmetric monounsaturated β_1 TAGs *versus* the symmetric ones (both see Part I).

It seems likely that the enlargement of the longest *d* spacing corresponds to a reduced interaction at the methyl end-plane, although this cannot be traced to specific enhanced contact distances. The reason is the limited resolution of the data that, as in the β_1 models, causes a poorly defined parallelism of the zigzig acyl-chain planes S1, S3 and O2*g*, as well as the total length of the chains.

4.6. The β_2 to β_1 phase transition

To transform a β_2 structure into a β_1 structure half of the three-packs have to be 'flipped over' along a line parallel to the *b* axis and in this transformation the inclined acyl-chain interface between the three-packs in β_2 has to change into the parallel interface found in β_1, which is energetically favourable. This 'flip over' does not seem easily realised in the solid state, but it is imaginable that liquidized top layers of β_2 crystallites can undergo such a transition, after which they may serve as β_1 seeds. In this way, it is comprehensible that slight cyclic heating and cooling promotes the β_2 to β_1 transition. This mechanism also complies with the results of re-crystallization experiments with cocoa butter (Van Langenvelde, Peschar & Schenk, 2001): when β-VI is melted to just a few degrees above its melting point and subsequently cooled, it re-crystallizes (fast) as β-VI. If the melting temperature is increased a few degrees more, upon cooling β-V recrystallizes, although much more slowly than β-VI. Melting beyond the so-called memory-point temperature does not yield any β crystallization upon cooling but only β' or lower melting polymorphs, depending on the crystallization temperature. Apparently, up to the memory point, the three-pack structure remains intact (dispersed) in the liquid state, but beyond this point the three-pack structures disintegrate. This mechanism is also consistent with seeding the liquid with a few tenths of a percent of a solid Sat-O-Sat'-type TAG (containing three-packs) at a temperature below the memory disappearance point, upon which the seeds 'restore' the original phase (Koyano *et al.*, 1990).

The occurrence of fat bloom on dark chocolate that accompanies the β-V to β-VI phase transition can now be understood in terms of three-pack structure migration and crystallization. At the rupture surface of a bloomed piece of dark chocolate, fat bloom is visible as a thin white layer. Using a light microscope the fat bloom layer locks the dark particles that color the bulk material (see supplementary material). A possible explanation is that the cocoa butter three-packs migrate to the surface and (re-)crystallize as β-VI while the coloring particles do not migrate. A migration that is enabled by the liquid state and is stimulated by a tempering process (cyclic heating and cooling) is also in line with analyses of fat bloom on dark non-bloomed chocolate that showed similar to slightly enhanced levels of POP, POS and SOS (Lonchampt & Hartel, 2004, and references therein), the principal components of the three-packs.

5. Conclusions

The structure determination results of the β_2 polymorphs and the previously solved β_1 polymorphs point out that structural imperfections are easily masked when data lack atomic resolution or when incorrect assumptions are made with respect to physical parameters. The option to model the presence of the preferred orientation can be useful but, apparently, has to be applied very carefully. In retrospect, even if the monoclinic cells would have been available at the time for β_2-SOS and β-V cocoa butter, it is unlikely that the current model would have been found. Essentially the same problems would have been encountered as during the structure determination of the β_1 polymorphs, which was not possible without human intervention.

The three-pack built-up of both the β_2 and β_1 polymorphs provides a simple explanation for the β_2 to β_1 phase transition and (re-)crystallization experiments of cocoa butter. Also, the occurrence of fat bloom can be understood as resulting from three-pack migration to the surface. In this respect, the discovery of the novel β_2 polymorphs of POS and SOA is of

interest since their crystallization seems attributable to the presence of three-packs of higher-melting TAGs that act as template seeds.

The enlargement of the longest axis seems related to a reduction of the melting point. A reduced interaction at the methyl end-plane seems likely, but could not be attributed unequivocally to specific increased interatomic contact distances because of the resolution of the data.

Based on the indexed β_2 and β_1 patterns, it could be established which reflections are responsible for the β-characteristic diffraction maxima in the fingerprint area. As the unit-cell parameters change anisotropically as a function of temperature, with the middle axis changing the most, and the peak positions also dependent on the chain length, the fingerprint area can only be interpreted completely if a reliable indexing is available.

The authors thank ADM Cocoa NL for providing the cocoa butter sample and Unilever Research Vlaardingen and Unilever Research Colworth for the pure triacylglycerols. The authors acknowledge the ESRF (Grenoble, France) for providing the facilities to perform the synchrotron diffraction experiments. The authors thank W. van Beek (Swiss–Norwegian CRG beamline BM01b) and E. Sonneveld (UvA) for their help in the collection of the β_2-POS, and I. Margiolaki (ID31), K. Goubitz (UvA) and R. B. Helmholdt (UvA) for their help in collecting data for β-V Ivory Coast. Dr V. Favre-Nicolin is gratefully acknowledged for proving several updated β versions of *FOX* with improved functionality. The investigations have been supported by the Netherlands Foundation for Chemical Research (NWO/CW) with financial aid from the Netherlands Technology Foundation (STW; project 790.350.405). The members of the User Committee of this project are thanked for stimulating discussions and continued interest.

References

De Jong, S., Van Soest, T. C. & Van Schaick, M. A. (1991). *J. Am. Oil Chem. Soc.* **68**, 371–378.
Dollase, W. A. (1986). *J. Appl. Cryst.* **19**, 267–272.
Favre-Nicolin, V. & Černý, R. (2002). *J. Appl. Cryst.* **35**, 734–743.
Helmholdt, R. B., Peschar, R. & Schenk, H. (2002). *Acta Cryst.* B**58**, 134–139.
Koyano, T., Hachyia, I. & Sato, K. (1990). *Food Struct.* **9**, 231–240.
Larson, A. C. & Von Dreele, R. B. (1987). *GSAS*. Report No. LA-UR-86-748. Los Alamos National Laboratory, New Mexico, USA.
Laugier, J. & Bochu, B. (2001). Chekcell; http://www.inpg.fr/LMPG.
Lonchampt, P. & Hartel, R. W. (2004). *Eur. J. Lipid Sci. Tech.* **106**, 241–274.
Lovegren, N. V. & Gray, M. S. (1978). *J. Am. Oil Chem. Soc.* **55**, 310–315.
Lovegren, N. V., Gray, M. S. & Feuge, R. O. (1976). *J. Am. Oil Chem. Soc.* **53**, 519–523.
March, A. (1932). *Z. Kristallogr.* **81**, 285–297.
Mechelen, J. B. van, Peschar, R. & Schenk, H. (2006). *Acta Cryst.* B**62**, 1121–1130.
Molecular Simulations Inc. (2000). *Cerius* Release 4.2. Biosym/Molecular Simulation Inc., San Diego, USA.
Peschar, R., Pop, M. M., De Ridder, D. J. A., Van Mechelen, J. B., Driessen, R. A. J. & Schenk, H. (2004). *J. Phys. Chem. B*, **108**, 15450–15453.
Sato, K., Arishima, T., Wang, Z. H., Ojima, K., Sagi, N. & Mori, H. (1989). *J. Am. Oil Chem. Soc.* **66**, 664–674.
Sprunt, J. C., Jayasooriya, U. A. & Wilson, R. H. (2000). *Phys. Chem. Chem. Phys.* **2**, 4299–4305.
Van Langevelde, A., Van Malssen, K., Peschar, R. & Schenk, H. (2001). *J. Am. Oil Chem. Soc.* **78**, 919–925.
Van Langevelde, A. J., Peschar, R. & Schenk, H. (2001). *Chem. Mater.* **13**, 1089–1094.
Yano, J., Ueno, S., Sato, K., Arishima, T., Sagi, N., Kaneko, F. & Kobayashi, M. (1993). *J. Phys. Chem.* **97**, 12967–12973.